**Proceedings of ASME Turbo Expo 2014: Turbine Technical Conference and Exposition**
**GT2014**
**June 16 – 20, 2014, Düsseldorf, Germany**

**GT2014-25992**

# ADIABATIC EFFECTIVENESS MEASUREMENTS FOR A BASELINE SHAPED FILM COOLING HOLE

**Robert P. Schroeder and Karen A. Thole**
Mechanical and Nuclear Engineering Department
Pennsylvania State University
University Park, PA 16802

## ABSTRACT

Film cooling on airfoils is a crucial cooling method as the gas turbine industry seeks higher turbine inlet temperatures. Shaped film cooling holes are widely used in many designs given the improved performance over that of cylindrical holes. Although there have been numerous studies of shaped holes, there is no established baseline shaped hole to which new cooling hole designs can be compared. The goal of this study is to offer the community a shaped hole design, representative of proprietary and open literature holes that serves as a baseline for comparison purposes. The baseline shaped cooling hole design includes the following features: hole inclination angle of 30º with a 7º expansion in the forward and lateral directions; hole length of 6 diameters; hole exit-to-inlet area ratio of 2.5; and lateral hole spacing of 6 diameters. Adiabatic effectiveness was measured with this new shaped hole and was found to peak near a blowing ratio of 1.5 at density ratios of 1.2 and 1.5 as well as at both low and moderate freestream turbulence of 5%. Reductions in area-averaged effectiveness due to freestream turbulence at low blowing ratios were as high as 10%.

## INTRODUCTION

Gas turbines utilize film cooling on hot gas path components to increase life by lowering metal temperatures. Cylindrical film cooling holes are the most economical to manufacture, but shaped holes have become widely used in military and commercial engines resulting from better cooling performance than cylindrical holes [1]. New novel cooling geometries are continually introduced as designers and researchers pursue better cooling performance. Cooling geometries that achieve higher cooling effectiveness with the same (or less) coolant are desirable because the compressor bleed air used for cooling can otherwise be used to produce power.

The impetus for the current study is the challenge in evaluating performance of any given cooling hole design. While there are many different shaped hole designs in literature, there are few geometries common between publications of different researchers. Most published film cooling studies compare novel cooling hole designs to the performance of a cylindrical hole, which is not necessarily the most helpful standard given the well-known jet detachment that occurs at high momentum flux ratios. The lack of one, single consensus baseline shaped hole currently limits the interpretation of cooling performance for new holes.

Designers and researchers would benefit from defining a baseline shaped hole geometry to be used instead of cylindrical holes for comparison purposes. This paper proposes a baseline shaped hole and presents adiabatic effectiveness data for the hole geometry at low and high density ratios and low and moderate freestream turbulence intensities. The design of the proposed baseline shape was guided by shaped holes in public literature while being representative of proprietary shaped hole designs. Data for this baseline shaped hole will be useful for evaluation of novel cooling hole geometries, benchmarking other investigations, and validation of CFD studies. The hole design and adiabatic effectiveness data in this paper are placed on a public website to share with the community (http://www.mne.psu.edu/psuexccl).

## NOMENCLATURE

| | |
|---|---|
| A | hole cross-sectional area |
| AR | area ratio, $A_{exit}/A_{inlet}$ |
| b | diameter of turbulence grid bars |
| $c_f$ | skin friction coefficient, measured experimentally |
| D | diameter of film cooling holes |
| DR | density ratio, $\rho_c/\rho_\infty$ |
| I | momentum flux ratio, $\rho_c U_c^2/\rho_\infty U_\infty^2$ |
| k | thermal conductivity |
| L | hole length |
| $\dot{m}_c$ | coolant mass flow rate |
| M | blowing ratio, $\rho_c U_c/\rho_\infty U_\infty$ |
| P | lateral distance between holes, pitch |
| R | radius of diffused outlet interior edges |
| Re | Reynolds number ($Re^* = \delta \cdot u_\tau/\nu_\infty$) |
| s | equivalent slot width based on metering area, $A_{inlet}/P$ |
| t | hole breakout width |
| T | temperature |
| Tu | freestream turbulence intensity, $u_{rms}/U_\infty$ |
| u | local streamwise velocity |

| | |
|---|---|
| $u_\tau$ | friction velocity, $U_\infty\sqrt{c_f/2}$ |
| $U_\infty$ | mainstream mean velocity |
| x | downstream distance measured from hole trailing edge |
| y | vertical distance from the surface |
| z | pitchwise distance measured from center hole |

**Greek**

| | |
|---|---|
| $\alpha$ | hole injection angle |
| $\beta$ | expansion angle for diffused outlet |
| $\gamma$ | effective injection angle, $\alpha - \beta_{fwd}$ |
| $\delta$ | 99% boundary layer thickness |
| $\eta$ | local adiabatic effectiveness, $(T_\infty-T_{aw})/(T_\infty-T_c)$ |
| $\theta$ | momentum thickness |
| $\Lambda_x$ | turbulence integral length scale |
| $\nu$ | kinematic viscosity |
| $\rho$ | fluid density |

**Subscripts**

| | |
|---|---|
| aw | adiabatic wall |
| c | coolant, at hole inlet |
| CL | centerline |
| eff | effective, at hole exit |
| exit | exit plane of the film cooling hole, per Figure 1 |
| fwd | forward expansion of shaped hole |
| inlet | inlet plane of the film cooling hole, per Figure 1 |
| lat | lateral expansion of shaped hole (half-angle) |
| m | metering section |
| $\infty$ | mainstream |

**Superscripts**

| | |
|---|---|
| $\bar{}$ | laterally-averaged |
| $\bar{\bar{}}$ | area-averaged |
| ’ | fluctuating/rms value |
| + | inner scaling coordinates |

## REVIEW OF RELEVANT LITERATURE

A review of shaped hole geometries found in the literature identified 130 different hole designs. Geometries included conical, laidback, and fanshaped holes [2-6], and many novel designs: bean-shaped [7], cusp-shaped [8], crescent-shaped [9], cratered [10], “Console” [11], double-jet [12], Nekomimi [13], transonic wall jet [14], waist-shaped [15], arrowhead-shaped [16], and anti-vortex holes [17]. The review included not only flat-plate studies, but also endwall, airfoil, and test coupon studies that featured shaped holes [18-20]. Far more studies were examined than can be reported in this paper, so a spreadsheet listing the studies and details of hole shapes is made available at the authors’ website [21]. The hole shape most frequent in literature was the laidback fanshaped, with over 50 variations identified for these laidback fanshaped holes.

Many of the shaped holes only differ from cylindrical holes by having a diffused outlet. The primary advantage of a diffused outlet is to decrease the momentum of the cooling jet at high flowrates relative to that of a cylindrical hole. By decreasing the momentum it reduces the jet penetration into the mainstream and reduces the likelihood of jet detachment [3].

Data for shaped film cooling holes were most recently tabulated and reviewed in the correlation developed by Colban et al. [22]. They found that effectiveness data collapsed better with blowing ratio (M) than with momentum flux ratio (I). Their correlation also accounted for pitchwise spacing (P/D), coverage ratio (t/P), and area ratio (AR). This correlation was successful in correlating laterally-averaged adiabatic effectiveness for shaped holes over a wide parameter range.

Shaped holes exhibit new flow phenomena in addition to that seen with cylindrical holes. Cooling jets from cylindrical holes detach from the surface at high momentum-flux ratios [23]. Jets from cylindrical holes also develop a counter-rotating vortex pair (CRVP, also called “kidney” vortices) that draws hot mainstream gas towards the surface [1]. With shaped holes, undesirable effects of the CRVP can be lessened through spreading apart the vortex pair and by formation of “anti-kidney” vortices [24]. Haven et el. [24] found that appearance of anti-kidney vortices depended on how the mainstream altered the windward side of the jet interface. Other flow phenomena includes a separation bubble that can form inside of the diffused outlet as observed by Saumweber and Schulz [5] causing a bimodal effectiveness pattern, which was also observed by Kampe et al. [25]. The separation inside the hole was result of expansion angles larger than 10º [5]. Large expansion angles in general cause jet separation inside the hole and thereby mainstream ingestion, as seen by Kohli and Bogard [4], Thole et al. [26], Lutum et al. [27], and Saumweber and Schulz [28].

At high coolant flowrates, different shaped holes can show different trends in cooling. For many shaped holes the effectiveness monotonically increases with blowing ratio and plateaus [22]. However, in other shaped holes effectiveness decreases as blowing ratio increases. Decreases have been observed to occur with holes having small expansion angles from 0º to 10º [5] and ironically with holes having large expansion angles thought to cause in-hole jet separation [4, 29].

Freestream turbulence is known to significantly affect film cooling in gas turbines, where turbulence intensity can be Tu = 20% exiting the combustor [30]. Bons et al. [31] measured performance of closely-spaced cylindrical holes at four turbulence intensities up to 17% and found that freestream turbulence was very effective in spreading coolant laterally. High freestream turbulence was observed to cause up to 70% reduction in centerline effectiveness at low momentum flux ratios. However, Bons et al. also found that at high momentum flux ratios with a detached jet, the change in centerline effectiveness from high freestream turbulence was negligible and effectiveness increased at the midpitch due to turbulence transporting coolant back onto the surface. Adiabatic effectiveness of shaped holes at moderate turbulence intensities up to Tu = 11% was measured by Saumweber et al. [32] and Saumweber and Schulz [28]. For shaped holes they observed no signs of jet detachment from the surface, and therefore freestream turbulence only acted to dilute the cooling and reduce adiabatic effectiveness. They saw a maximum decrease of 30% in laterally-averaged effectiveness at low blowing ratios, due to freestream turbulence increasing from Tu = 3.6% to 11% [32]. Colban et al. [18] observed smaller reductions in effectiveness for shaped holes on a turbine endwall. When

incoming freestream turbulence was increased from Tu = 1.2% to 8.9%, area-averaged adiabatic effectiveness with shaped holes decreased an average of 6%.

In reviewing the film cooling literature, it was found that there is no standard shaped cooling hole for new holes to be compared with. Moreover, there are conflicting trends in the results for the various film cooling hole shapes. The hole proposed in this paper is presented as a standard shaped hole for the community to compare with. This paper is the first in a series that will be presented in which a full documentation of the surface cooling, flow and thermal fields, and various effects such as curvature, pressure gradients, and hole roughness will be presented.

## DESIGN OF THE BASELINE SHAPED HOLE

The authors chose the laidback fanshaped hole as the geometry for the baseline shaped hole, due its predominance in the literature and use in industry. Table 1 summarizes the ranges for geometric parameters commonly found in the literature for laidback fanshaped holes. These geometric features served as a guide for designing the baseline shaped hole. In the literature there was a large variety in hole shapes. Interestingly many geometries had short metering sections that take up half or less of the total length of the shaped hole, which contradicts the suggested design [1] that the diffused outlet is confined to the "outer 20-50% of the wall thickness."

The design chosen for the baseline shaped hole is described by the geometric parameters in the rightmost column of Table 1. This exact hole shape is illustrated in Figure 1 and is available for download from the authors' website [21]. As illustrated at the bottom of Figure 1, the diffused outlet shape is driven by guidelines from the circular end of the metering section (plane A-A) to the filleted rectangle of plane B-B. The expansion angle in each direction was 7º, hence the name "7-7-7 shaped hole." Lateral expansion angle is defined from the metering section axis as in Figure 1, with the half-angle being 7º and therefore the full-angle being 14º. The expansion angle of 7º is seen in literature with the research by Fawcett et al. [33] who had a 7º forward expansion, and in Gritsch et al. [3] who tested multiple shaped holes with 7º lateral expansion. The length of the metering section was chosen to be $L_m/D = 2.5$ or 42% the total length of the hole, which is representative of shaped holes reviewed. The hole length and 7º expansion angles resulted in an area ratio AR = 2.5.

Overall the design choices differentiated the 7-7-7 baseline shaped hole from the geometry investigated extensively by Wittig and coworkers [26, 32, 34-37]. They investigated the performance of fanshaped and laidback fanshaped holes having 15º forward expansion and 14º lateral expansion (half-angle; verified to have been defined as in Figure 1). Expansion angles for the 7-7-7 shaped hole are about half those of Wittig, which helps ensure the baseline shaped hole performance will not be complicated by jet separation inside the hole [26, 28, 34] or bimodal effectiveness patterns [5]. Also different is that the forward expansion of the 7-7-7 shaped hole begins well towards the entrance of the hole, which allows forward diffusion prior to interaction with the mainstream. One commonality between the 7-7-7 shaped hole and those studied by Wittig is that in-hole edges of the diffused outlet are rounded to R/D = 0.5. For brevity, the 7-7-7 baseline shaped hole will henceforth in this paper be referred to as the "shaped hole."

**Table 1. Geometric Parameters for Baseline Shaped Hole**

| | Range Common in Literature | 7-7-7 Shaped Hole |
|---|---|---|
| Injection Angle, $\alpha$ | 30 to 55º | 30º |
| $L_m/D$ | 1 to 4 | 2.5 |
| $L_{lat}/D$, $L_{fwd}/D$ | 1.6 to 9.5 | 3.5 |
| L/D | 2.8 to 11.5 | 6 |
| Laidback Angle, $\beta_{fwd}$ | 2 to 25º | 7º |
| Lateral Angle, $\beta_{lat}$ | 2 to 18º | 7º |
| P/D | 2.8 to 8 | 6 |
| Coverage Ratio, t/P | 0.3 to 0.8 | 0.35 |
| Area Ratio, AR | 2.5 to 4.7 | 2.5 |
| Sharpness of Inlet and Breakout Edges | Usually Sharp | Sharp |
| Rounding of Four Edges Inside Diffuser, R/D | 0 to 0.5 | 0.5 |

## EXPERIMENTAL FACILITY

Adiabatic effectiveness measurements were acquired in a closed-loop wind tunnel shown in Figure 2 that was previously described by Eberly and Thole [38]. Mainstream air was circulated by an in-line centrifugal fan. For our study, the mainstream temperature was maintained at 295 K with a bank of electrical heating elements and a chilled water heat exchanger. As shown in Figure 2, the incoming boundary layer was removed with a suction loop at the entrance of the test section. A new boundary layer originated at the leading edge of the test plate and a trip wire at x/D = -35 initiated transition of the boundary layer to a turbulent state.

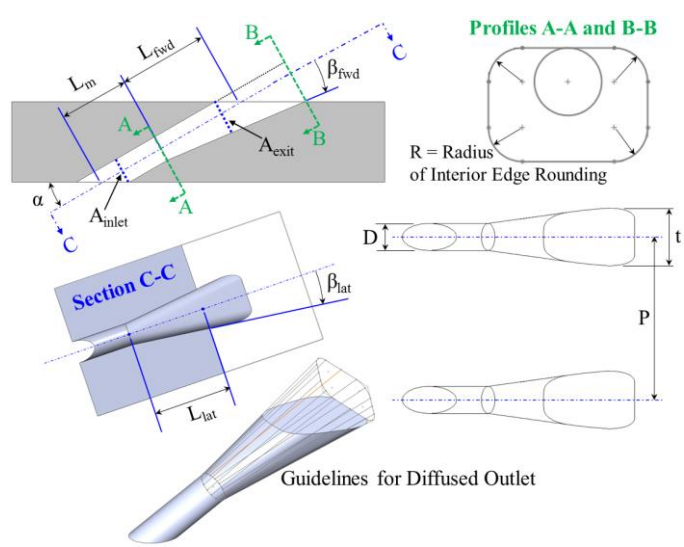


**Figure 1. Baseline shaped hole design.**

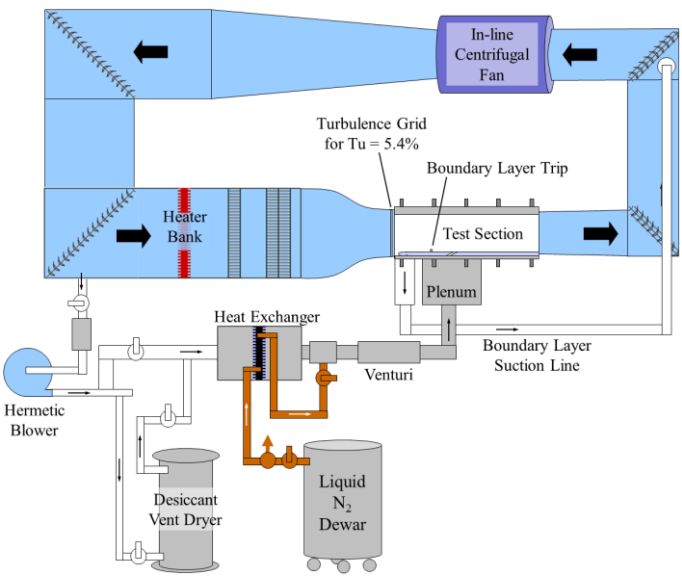


**Figure 2. Schematic of wind tunnel used in current study.**

Coolant air for the film cooling injection was diverted from the mainstream using a variable frequency blower that was hermetically sealed. To avoid frost formation that can result from cryogenically cooling the coolant, the coolant was routed through a vent dryer containing solid desiccant. Downstream of the heat exchanger and prior to entering the plenum, the coolant flowrate was measured with a Venturi flow meter. Three flow conditioning screens inside the plenum were used to ensure uniformity of flow to the film cooling holes.

Film cooling holes were machined in Dow Styrofoam brand residential sheathing (k = 0.029 W/m·K) to ensure a nearly adiabatic surface for effectiveness measurement. The film cooling array was a row of five shaped holes with a metering diameter of 7.75 mm. Adiabatic effectiveness measurements were determined from surface temperature measurements made with a FLIR SC620 infrared camera. The camera output was calibrated to accurately detect the entire range of temperatures measured, similar to as done by Eberly and Thole [38]. Coolant and freestream temperatures were each measured using multiple thermocouples. Adiabatic effectiveness measurements made by Eberly and Thole for cylindrical holes in this facility showed good agreement with the literature [38].

## UNCERTAINTY ANALYSIS

An uncertainty analysis was performed for variables of density ratio, blowing ratio, and adiabatic effectiveness by propagating uncertainties using partial derivatives as outlined by Figliola and Beasley [39]. All calculations were done for a 95% confidence interval.

Uncertainty in density ratio was found to be low, being less than ±0.01 and ±0.02 for DR = 1.2 and 1.5 respectively. Blowing ratio uncertainty was found to be highest at the lowest blowing ratio of M = 0.5, for the worst case being ±10% (DR = 1.5, M = 0.5). The uncertainty in M = 0.5 was result of bias uncertainty in the Venturi flowmeter itself (±0.25% of full-scale flow and verified by separate tests with a laminar flow element in series). As coolant flowrate increased, percent uncertainty in M decreased because the inherent flowmeter uncertainty became less dominant. Maximum uncertainty for blowing ratios M = 2 and above was ±2.9%.

The uncertainty in adiabatic effectiveness was found to be greater at DR = 1.2 than at DR = 1.5 because of the smaller $\Delta T$ between the coolant and mainstream. Uncertainty in surface temperature (±0.9 ºC for DR = 1.2, ±1.8 ºC for DR = 1.5) was based on scatter in the infrared camera calibration data and bias uncertainty of the thermocouples used in the calibration, both of which became larger at lower temperatures. Uncertainty in coolant temperature accounted for variation between plenum thermocouples near the cooling holes. This variation was greatest at blowing ratio M = 0.5. Adiabatic effectiveness uncertainty was calculated to be $\delta\eta = \pm 0.031$ for DR = 1.2 and $\delta\eta = \pm 0.024$ for DR = 1.5. Repeatability was confirmed to within the uncertainty by repeating the measurements over a four month period with a separate foam specimen giving a maximum difference in laterally-averaged effectiveness of $\Delta\bar{\eta} = 0.025$, which was within the uncertainty range.

## TEST MATRIX AND APPROACH FLOW CONDITIONS

Table 2 summarizes the test conditions used for the adiabatic effectiveness measurements, which included low and moderate freestream turbulence. Freestream turbulence intensity (Tu) is reported for the hole injection location and blowing ratio and jet Reynolds number ($Re_D$) are evaluated at the metering section of the hole. The mainstream velocity was 10 m/s for all tests.

**Table 2. Test Matrix**

| Tu | DR | Blowing Ratios | $Re_D$ |
|---|---|---|---|
| 0.5% | 1.2 | M = 0.5, 1, 2, 3 | 2800 - 16900 |
| 0.5% | 1.5 | M = 0.5, 1, 1.5, 2, 2.5, 3 | 3400 - 20600 |
| 5.4% | 1.5 | M = 0.5, 1, 2, 3 | 3400 - 20600 |

Moderate freestream turbulence of Tu = 5.4% was obtained by installing a vertical-bar turbulence grid upstream of the flat plate leading edge at x/D = -69. The grid was composed of vertical round bars of diameter b = 9.5 mm, spaced 25.4 mm apart center-to-center. Laser Doppler Velocimetery (LDV) was used to characterize the freestream turbulence downstream of the grid. The turbulence intensity of 5.4% is reported for the hole trailing edge position (x/D = 0), which decayed to 4.4% at x/D = 22. Turbulence intensity and its decay with streamwise distance agreed well with the parallel-rod correlation of Roach [40]. For Tu = 5.4% at x/D = 0, the integral length scale was estimated to be $\Lambda_x/D = 2.2$ based on measurements reported with an identical grid geometry [41].

The approach turbulent boundary layer was measured at x/D = -4.7 for both low and moderate freestream turbulence. Boundary layers were measured for at least five pitchwise locations and average values are presented in Table 3. Profiles of mean and fluctuating velocity at z/D = 0 are given in Figures 3 and 4, respectively.

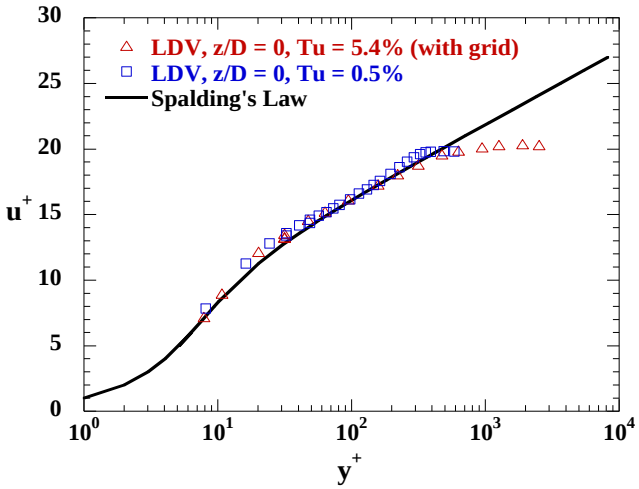


**Figure 3. Turbulent boundary layers measured at x/D = -4.7, with and without the upstream turbulence grid.**

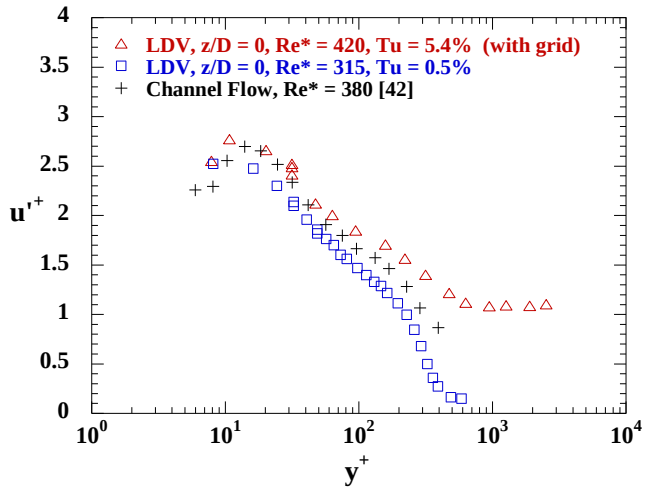


**Figure 4. Profiles of streamwise velocity fluctuation at x/D = -4.7, with and without the upstream turbulence grid.**

**Table 3. Characteristics of Approach Boundary Layer**

| Tu | θ/D | H | $Re_\theta$ | Re* | $u_\tau$ |
|---|---|---|---|---|---|
| 0.5% | 0.14 | 1.45 | 670 | 315 | 0.5 m/s |
| 5.4% | 0.28 | 1.3 | 1380 | 420 | 0.5 m/s |

## ADIABATIC EFFECTIVENESS AT LOW TURBULENCE

Contours of adiabatic effectiveness for DR = 1.2 at low freestream turbulence are shown in Figure 5 for three cooling holes in the center of the array. The contours show good periodicity between the three holes and, although it is not shown here, good periodicity was achieved with all five holes. Note that the values inside the holes are not given due to the camera focal location being on the flat plate surface.

At low blowing ratios, increases in the coolant flowrate from M = 0.5 to M = 1 resulted in increases in the adiabatic effectiveness. At flowrates above M = 1, Figure 5 shows that coolant patterns on the surface began to narrow and continued to do so as the blowing ratio increased. Figure 6 gives the laterally-averaged effectiveness for the DR = 1.2 cases using the averaged values for the three holes shown in the contours. The highest effectiveness was at M = 1. Notice that far from the holes the decay rate was slower for the higher blowing ratios.

Figure 7 shows adiabatic effectiveness contours for the same four blowing ratios at the higher density ratio of DR = 1.5. As was seen at DR = 1.2, effectiveness increased and then began to decrease with increasing blowing ratio

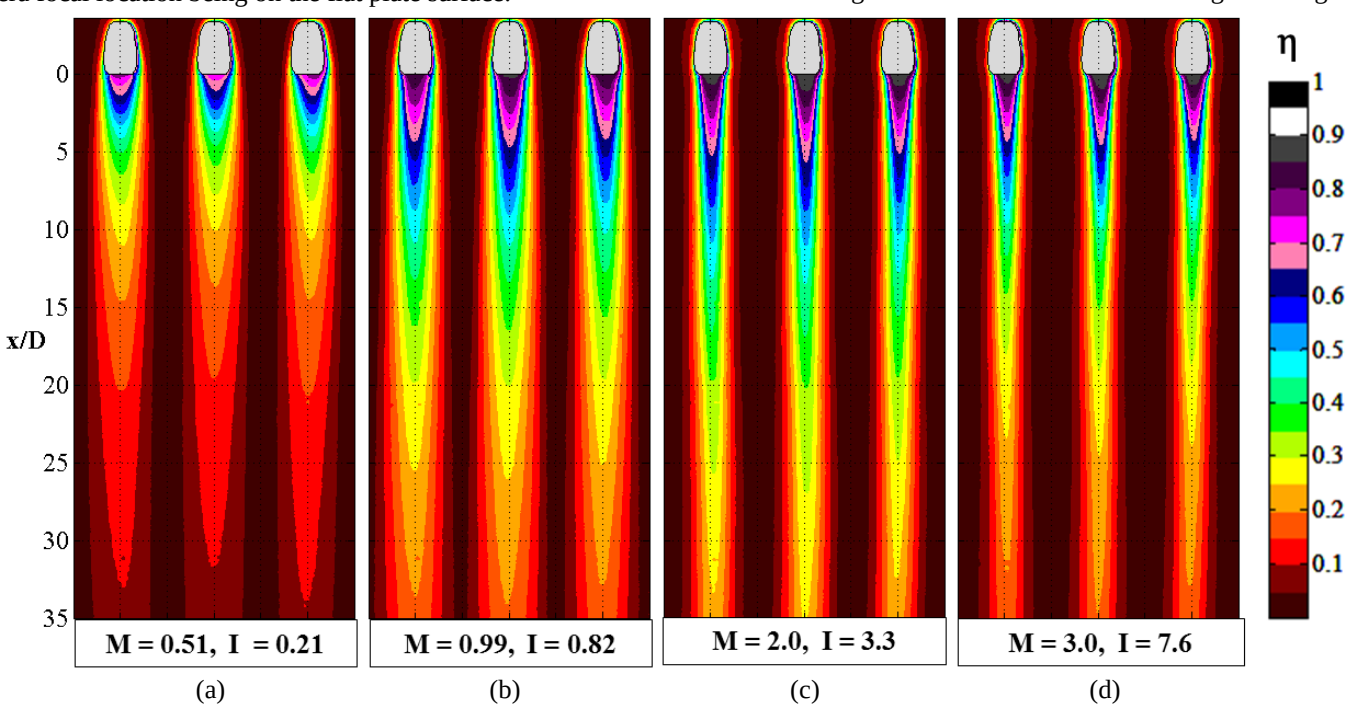


**Figure 5. Shaped hole η contours for DR=1.2, low freestream turbulence: (a) M=0.5, (b) M=1, (c) M=2, and (d) M=3.**

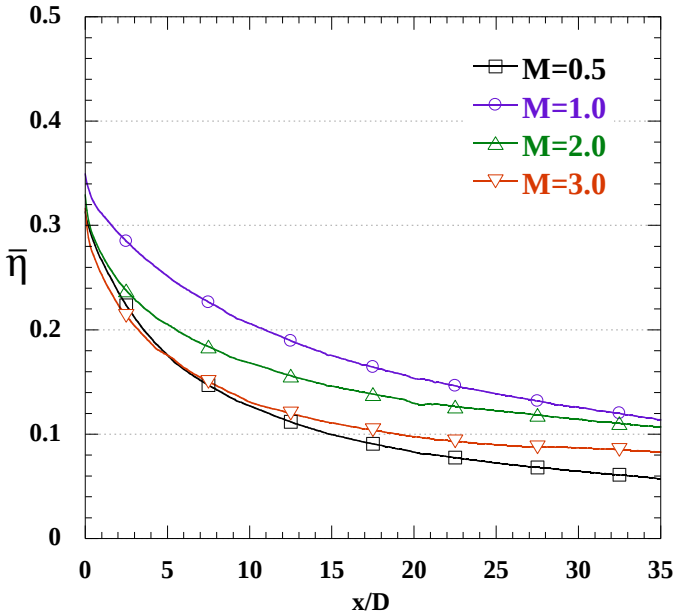


**Figure 6. Shaped hole laterally-averaged effectiveness at DR=1.2, low freestream turbulence.**

resulting from the narrowing of the jet. At blowing ratios above M = 1, the coolant footprint progressively narrowed with increases in blowing ratio. Centerline effectiveness values for all DR = 1.5 cases are given in Figure 8a (note not all the contours were presented in Figure 7 for brevity). The results show how the behavior changed from low blowing ratio to high blowing ratio. At the trailing edge of the hole, centerline effectiveness increased with blowing ratio until plateauing at M = 1.5. The lower centerline effectiveness at the trailing edge for M = 0.5 and 1 can be explained by mainstream ingestion occurring when coolant had low momentum ($I_{eff}$ = 0.03 and 0.11 respectively, calculated from $I_{eff} = I/AR^2$). Thole et al. [26] observed mainstream ingestion into a laidback fanshaped hole at $I_{eff}$ = 0.25. Mainstream ingestion caused mixing that diluted the coolant inside the diffused outlet. At higher blowing ratios, coolant had more momentum and resisted mainstream ingestion. Laterally-averaged effectiveness shown in Figure 8b also indicates a change in behavior at M = 1.5. For x/D > 5, the highest laterally-averaged effectiveness occurred at M = 1.5 which also exhibited a slower decay in $\bar{\eta}$ than at M = 0.5 or 1. The steeper decay in effectiveness at low blowing ratios was attributed to mainstream ingestion. At blowing ratios greater than M = 1.5 the decay in effectiveness remained slow.

Laterally-averaged effectiveness was found to be higher at the high density ratio for the same blowing ratio, which resulted from an increased lateral spreading of the coolant. Figure 9 compares laterally-averaged effectiveness between DR = 1.2 and 1.5. In Figure 9 the solid symbols are the high density ratio data. Increased effectiveness at high density ratio was associated with better lateral spreading of the coolant jet at high density ratio, consistent with observations by Eberly and Thole for cylindrical holes [38]. Figure 10 shows lateral distributions of coolant for the center pitch at M = 1 and 3. At x/D = 5 (Figure 10a) the increased spreading at DR = 1.5 was only slightly apparent. Lateral spreading increased with downstream distance, as evidenced by lateral distributions at x/D = 30 (Figure 10b). At both blowing ratios, the lateral spread of the coolant was greater at DR = 1.5 than at DR = 1.2. Note the vertical scale is reduced in Figure 10b to show detail.

Scaling of adiabatic effectiveness with blowing ratio and momentum flux ratio was investigated. Since effectiveness for cylindrical holes is known to scale with blowing ratio in the regime where jets do not detach from the surface [23], it is

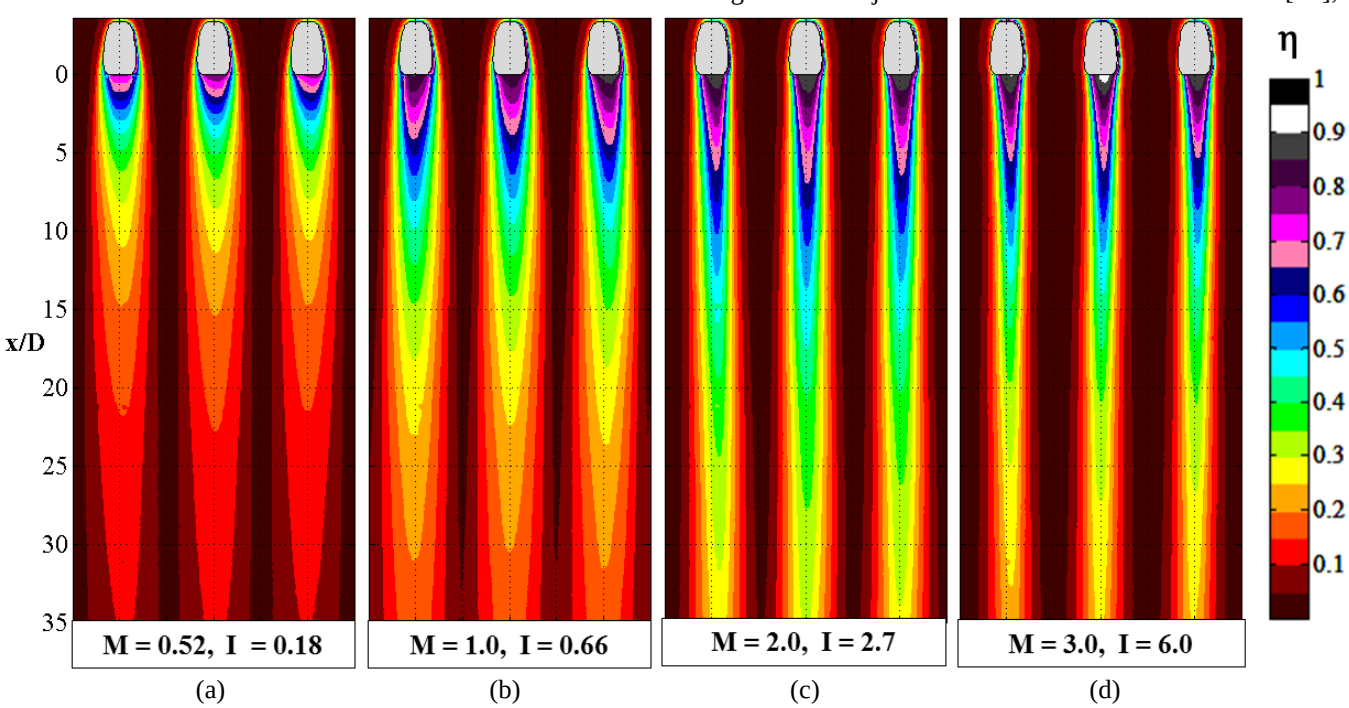


**Figure 7. Shaped hole η contours for DR=1.5, low freestream turbulence: (a) M=0.5, (b) M=1, (c) M=2, and (d) M=3.**

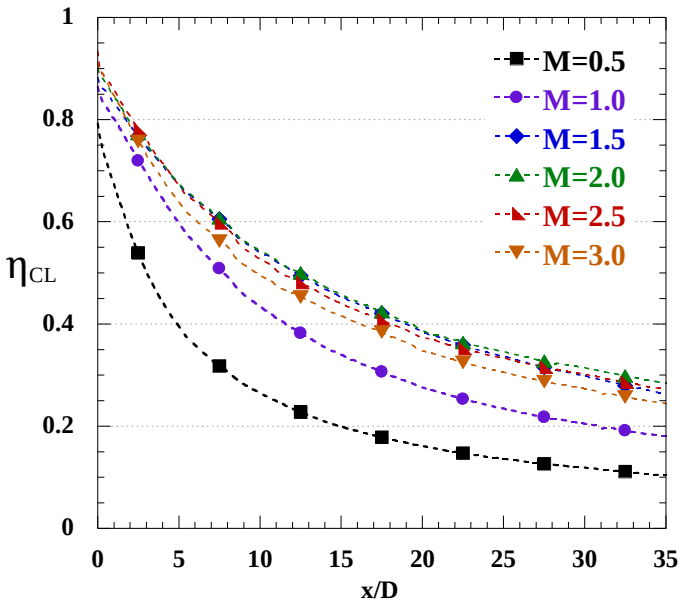


**Figure 8a. Shaped hole centerline effectiveness at DR=1.5, low freestream turbulence.**

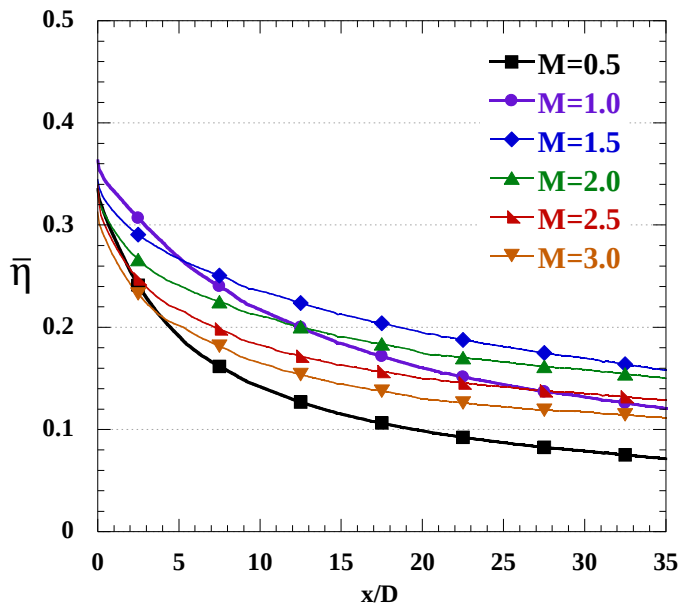


**Figure 8b. Shaped hole laterally-averaged effectiveness at DR=1.5, low freestream turbulence.**

plausible that the attached jets from shaped holes would scale similarly. Effectiveness averaged over the three hole pitches over a streamwise distance between $3 \leq x/D \leq 35$ is shown in Figure 11 for both density ratios. (Predictions from the correlation of Colban et al. [22] are also shown and will be discussed in the following section.) At low blowing ratios, the DR = 1.2 and 1.5 results for the shaped hole indicated similar effectiveness. The $\bar{\bar{\eta}}$ curves did not collapse, however, at blowing ratios $M \geq 2$ because of the better cooling achieved at DR = 1.5 compared with 1.2.

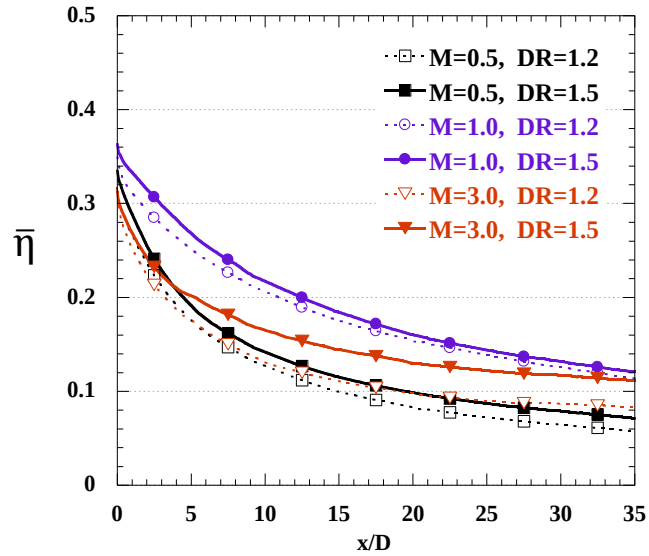


**Figure 9. Comparison of laterally-averaged effectiveness at DR=1.2 and DR=1.5, low freestream turbulence.**

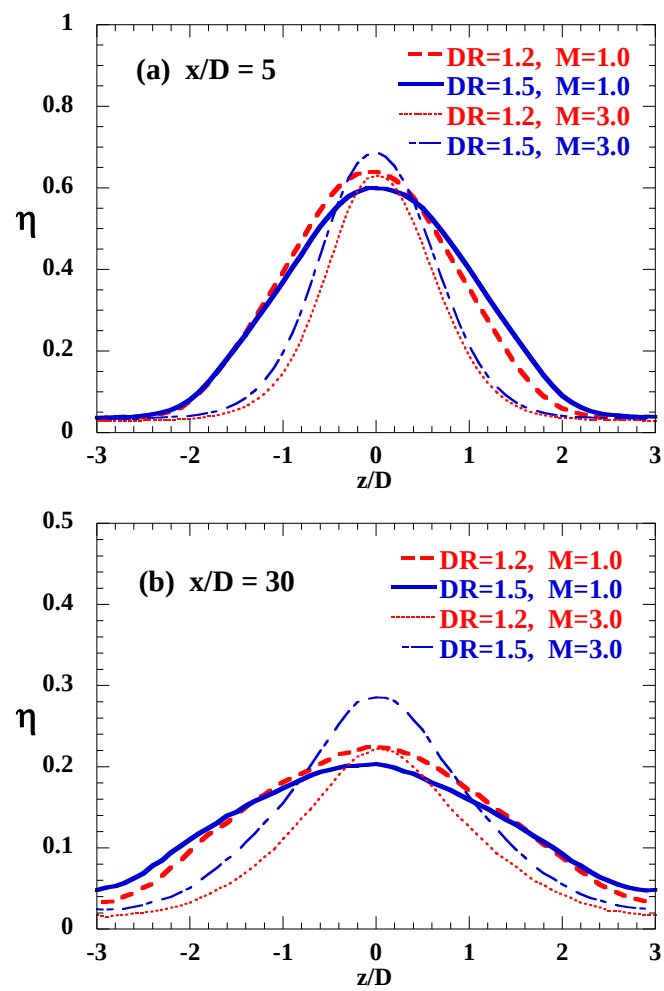


**Figure 10. Lateral distributions of effectiveness compared between DR=1.2 and 1.5, at M=1.0 and 3.0, Tu=0.5% for (a) x/D=5 and (b) x/D=30. Center pitch shown.**

Figure 12 shows the same area-averaged effectiveness as a function of momentum flux ratio. The top abscissa in Figure 12 is the effective momentum flux ratio occurring at the hole exit, $I_{eff}$. At DR = 1.5 the peak effectiveness occurred at $I_{eff} = 0.2$. Above $I_{eff} = 0.2$, the area-averaged effectiveness did not collapse very well at the two density ratios. In summary, effectiveness for the shaped holes did not scale with blowing ratio or momentum flux ratio over the whole range evaluated.

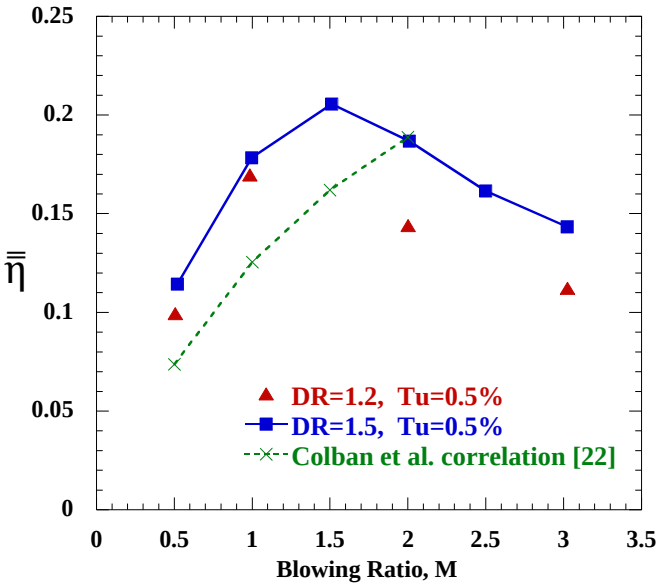


**Figure 11. Area-averaged effectiveness for shaped holes plotted as a function of the blowing ratio. Averaged over x/D = 3-35.**

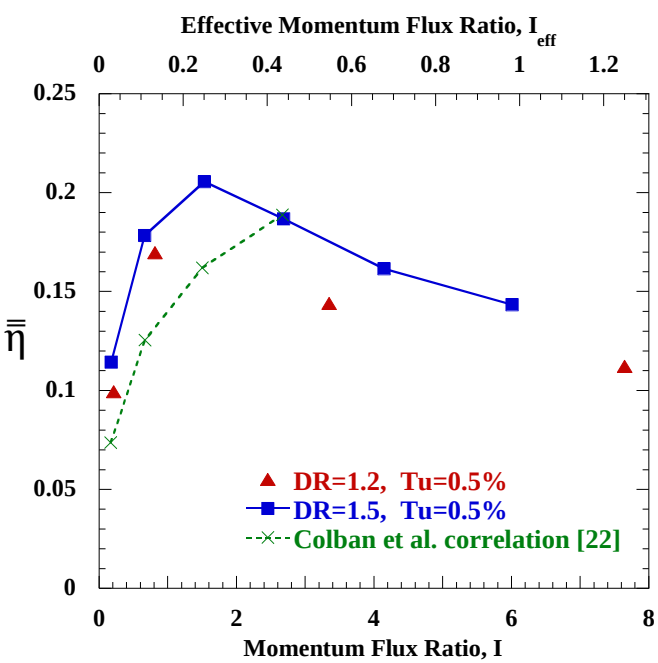


**Figure 12. Area-averaged effectiveness for shaped holes plotted as a function of the regular and effective momentum flux ratios. Averaged over x/D = 3-35.**

## PERFORMANCE RELATIVE TO OTHER GEOMETRIES

Comparisons of the results were made to the shaped hole correlation of Colban et al. [22] developed for film cooling at density ratios between $1.7 \leq DR \leq 2$. Figure 13 compares laterally-averaged effectiveness measured at DR = 1.5 in the current study to the correlation. The shaped hole correlation underpredicted effectiveness for blowing ratios below M = 2. At M = 2, agreement between the correlation and the current study was relatively good. Higher blowing ratios are not plotted because they correspond to parameter values outside those used to develop the correlation. Effectiveness predicted from the correlation was area-averaged and is given in Figures 11 and 12 as mentioned earlier. As seen, the correlation underpredicted the DR = 1.5 $\bar{\bar{\eta}}$ at blowing ratios up to M = 2.

The disagreement between the current study and the correlation may be attributed to the 18 different shaped holes used to develop the correlation as shown in Table 4. Table 4 compares the shaped hole of the current study to three holes used in developing the correlation (Saumweber et al. [32], Colban et al. [22], and Gritsch et al. [3]). The shaped hole of the current study was at the low extreme of area ratios

**Table 4. Comparison of Shaped Holes**

| | $L_m$ /D | $L_{lat}$ /D | $L_{fwd}$ /D | $\beta_{lat}$ | $\beta_{fwd}$ | R/D | α | P/D | t/P | AR |
|---|---|---|---|---|---|---|---|---|---|---|
| Current Study | 2.5 | 3.5 | 3.5 | 7º | 7º | 0.5 | 30º | 6 | 0.35 | 2.5 |
| Saumweber et al. [32] | 2 | 4 | 1 | 14º | 15º | 0.5 | 30º | 4 | 0.75 | 3.1 |
| Colban et al. [22] | ≥ 2* | 4* | 4* | 10º | 10º | 0.5 | 30º | 6.5 | 0.48 | 3.9 |
| Gritsch et al. [3] | 2 | 9.5 | 9.5 | 2º | 4º | >0.5* | 30º | 6 | 0.31 | 2.5 |
| Heneka et al. [6] | 2 | 3.5* | 3.5* | 10º | 10º | 0 | 35º | 8 | 0.37 | 3.7 |

* -- value approximated from information provided in reference

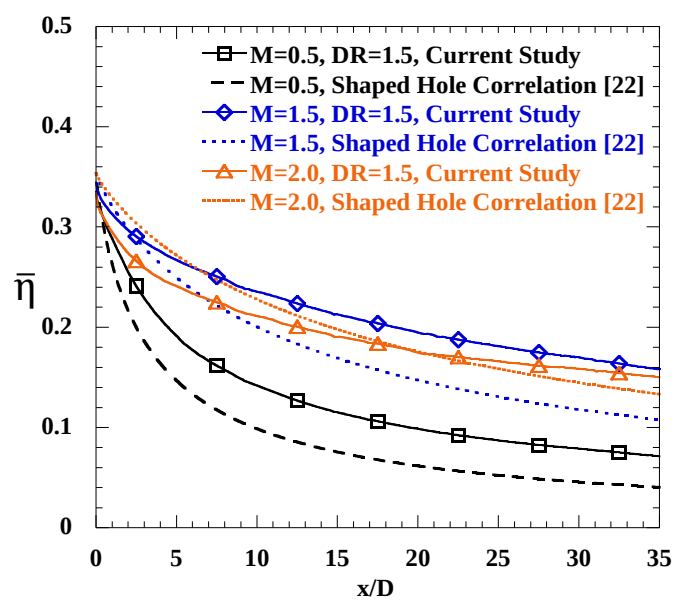


**Figure 13. Laterally-averaged adiabatic effectiveness in the current study compared to predictions from the shaped hole correlation [22].**

incorporated into the correlation, as only 3 of the 18 shaped holes had AR = 2.5 and none of the 18 had lower area ratios. Additionally, the majority of the shaped holes used to develop the correlation had diffused outlets much longer than in the current study. Most of the shaped holes used to develop the correlation were those presented by Gritsch et al. [3], comprising 13 of the 18 hole shapes used to derive the correlation [22]. All 13 of these shaped holes had diffused outlets at least 5.5D long. Longer diffused outlets lead to different exiting velocity profiles which in turn affects adiabatic effectiveness. Differences in the exact shape of the hole breakout may also have had influence. Haven et al. [24] found that breakout shape affects the counter-rotating vortex pair, since the leading edge of the breakout influences how the jet-mainstream interface is deformed. The schematic in Gritsch et al. [3] shows that their shaped hole breakouts had a bowed leading edge, as compared to the straight leading edge of the shaped hole for the current study (see Figure 1).

The shaped hole of the current study has expansion angles and an area ratio less-aggressive than several other shaped holes in literature, so a reasonable question is where performance falls with respect to other shaped holes. Figure 14 compares cooling performance in the current study to that of the shaped holes listed in Table 4, all of which are laidback fanshaped holes. The vertical axis gives area-averaged effectiveness, taken over the range x/D = 5-22 available from these studies. An exception is that Saumweber et al. [32] reported $\bar{\bar{\eta}}$ over x/D = 2-22. The geometries had pitchwise spacings varying from P/D = 4-8, but were made comparable by plotting as a function of a scaled blowing ratio as massflow per unit pitch. This variable is normalized by mainstream variables and the hole diameter as shown in Equation 1.

$$\frac{(\dot{m}_c / P)}{\rho_\infty U_\infty \cdot D} = \frac{(\dot{m}_c / A_{inlet})}{\rho_\infty U_\infty} \cdot \frac{A_{inlet}/P}{D} = M \cdot \frac{s}{D} \qquad (1)$$

At low values of M·s/D Figure 14 shows that film cooling holes tend to the same performance regardless of shaped hole geometry differences. At high values, the shaped hole of Heneka et al. [6] performed worst among the shaped holes with their hole having the highest injection angle (α). Heneka et al. hypothesized that the low effectiveness may be related to sharp edges of their holes (R/D = 0) perhaps initiating detrimental vortices inside the shaped hole.

It is worthwhile to note that higher $\bar{\bar{\eta}}$ corresponded closely with the effective angle of diffused injection as mentioned by Saumweber and Schulz [5]. The effective angle of diffused injection (γ) is given by the angle between the diffuser floor of the hole and the external surface. It appears that shallower angles lead to greater cooling as shown in Figure 14. The shaped hole of the current study had an effective injection angle of 23º, which was relatively steep among the laidback fanshaped holes. It is also interesting to see that for shallower angles below 20º the cooling performance increases with M·s/D as compared with angles greater where increases in M·s/D result in decreased cooling. The authors note that not all

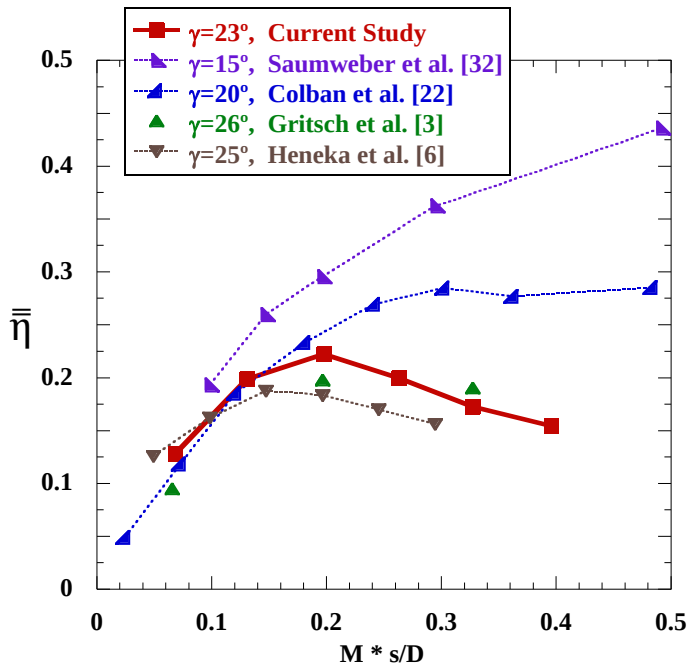


**Figure 14. Area-averaged effectiveness for shaped holes at high density ratio and low freestream turbulence, plotted as a function of the coolant flowrate per pitch (Equation 1).**

shaped holes scale in this manner with only the effective injection angle.

## ADIABATIC EFFECTIVENESS AT MODERATE TURBULENCE

With the turbulence grid installed, adiabatic effectiveness was measured for the shaped holes at DR = 1.5. Contours of effectiveness measured at moderate turbulence are shown in Figure 15. In comparing Figure 15 with Figure 7, it is seen that the freestream turbulence increased mixing between coolant and the mainstream, particularly evident on jet centerlines at low blowing ratios. At each blowing ratio, centerline effectiveness decreased with increased freestream turbulence. Mixing from increased freestream turbulence also manifested itself as increased lateral spreading of coolant relative to Tu = 0.5%, except at M = 0.5. Negligible coolant spreading occurred at M = 0.5 when comparing the low and moderate turbulence intensities. At M = 1 and M = 2, the η = 0.05 contour level for adjacent jets merged by x/D = 25. At M = 2 and 3, narrowing of coolant footprints similar to the low freestream turbulence occurred with the moderate freestream turbulence.

Figure 16 compares laterally-averaged effectiveness at low and moderate freestream turbulence intensities. For M = 0.5 and 1, the increased freestream turbulence decreased $\bar{\eta}$ relative to the low turbulence case. At M = 2 and 3 the effect of increased freestream turbulence on $\bar{\eta}$ was nearly negligible. The effect of increasing freestream turbulence is revealed by lateral effectiveness distributions at Tu =0.5% and 5.4% shown in Figure 17. Note the scale was reduced in Figure 17b as

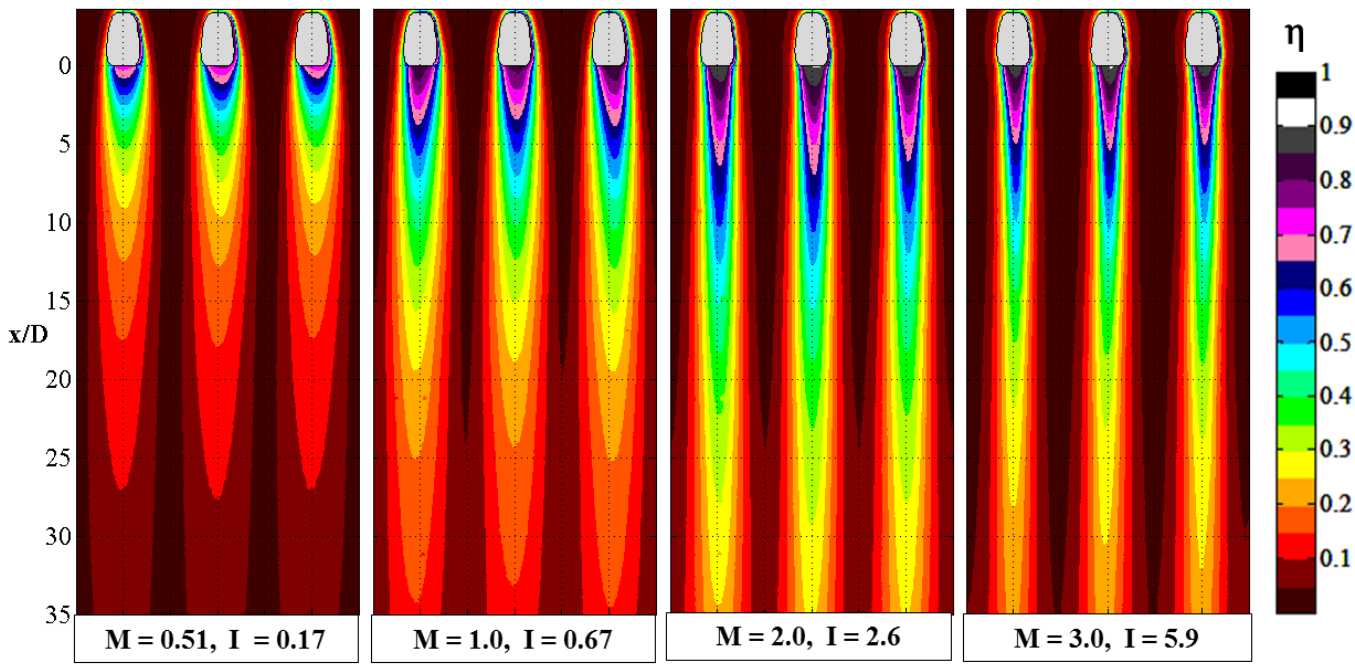


(a) (b) (c) (d)

**Figure 15. Shaped hole η contours at DR=1.5, moderate freestream turbulence: (a) M=0.5, (b) M=1, (c) M=2, and (d) M=3.**

compared with Figure 17a to show the details. Near the hole at x/D = 5, increased freestream turbulence did not change the lateral spreading of coolant. Far downstream of the holes at x/D = 30, as shown in Figure 17b, the coolant footprint at M = 3 was widened by the freestream turbulence but not so for M = 1. Freestream turbulence also caused reduction in centerline effectiveness relative to the Tu = 0.5% performance.

The effect of freestream turbulence on area-averaged effectiveness is shown in Figure 18. Area-averaging was done over the range x/D = 2-22 for comparison of the current study to shaped hole freestream-turbulence results from Saumweber et al. [32]. Figure 18 shows that at blowing ratios M = 0.5 and 1 in the current study, increased freestream turbulence of Tu = 5.4% led to reductions in $\bar{\bar{\eta}}$ of up to 10%. At higher blowing ratios, the freestream turbulence caused no reduction in $\bar{\bar{\eta}}$. In the study of Saumweber et al. [32], increasing freestream turbulence from Tu = 3.6% to 7.5% led to similar reductions (11%) in $\bar{\bar{\eta}}$ at low blowing ratios. However, at high blowing ratios the percent reductions were 5-10%. The results of the current study are consistent with observations by Colban et al. [18] for shaped holes on an endwall. Most of the holes on the endwall were operating at blowing ratios below M = 2, and laterally-averaged effectiveness only decreased slightly or remained unchanged when freestream turbulence was elevated from Tu = 1.2% to 8.9%. Area-averaged effectiveness on the endwall decreased an average of 6% from the elevated freestream turbulence.

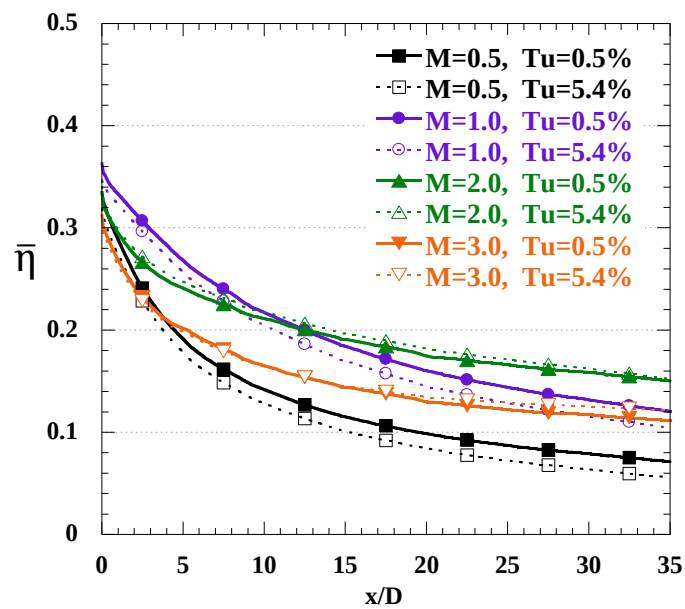


**Figure 16. Comparison of DR=1.5 laterally-averaged effectiveness at low and moderate freestream turbulence.**

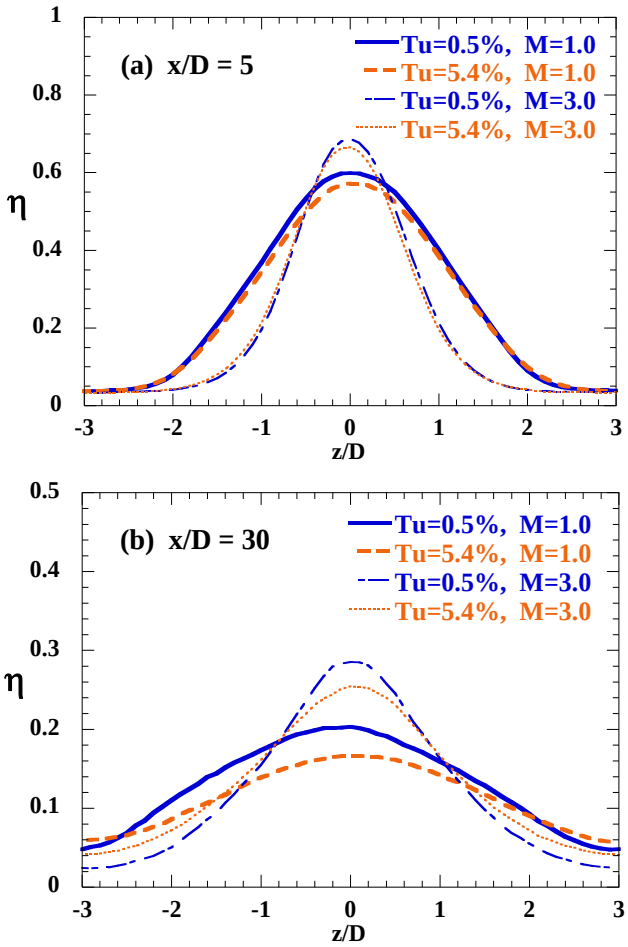


**Figure 17. Lateral distributions of effectiveness compared between Tu=0.5% and 5.4%, at M=1.0 and 3.0, DR = 1.5 for (a) x/D=5 and (b) x/D=30. Center pitch shown.**

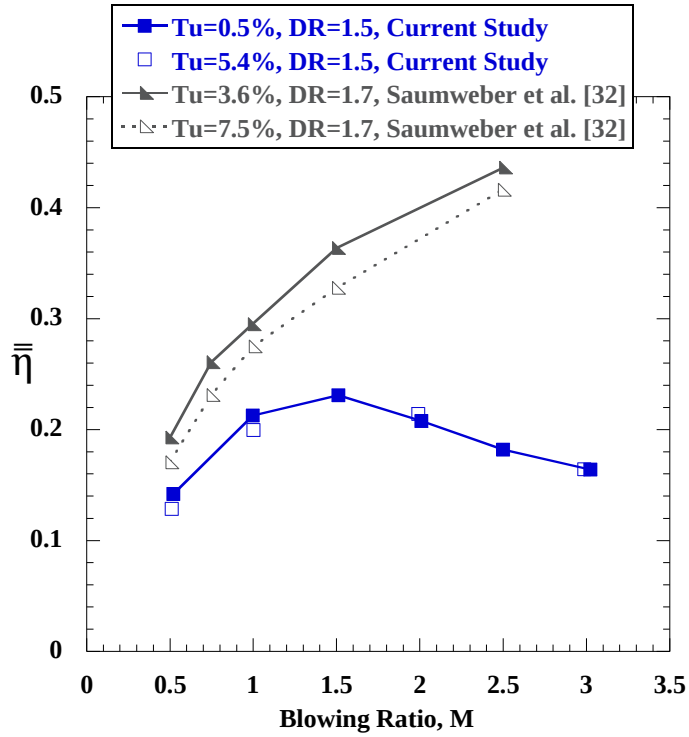


**Figure 18. Area-averaged effectiveness for shaped holes plotted as a function of the blowing ratio. Averaged over x/D = 2-22.**

## CONCLUSIONS

A baseline shaped hole was designed after reviewing shaped holes in public literature and their performance characteristics. Geometric parameters for the shaped hole match those seen with shaped holes in literature. Conservative expansion angles of 7º were selected so this shaped hole would not exhibit in-hole jet separation. The geometric parameters resulted in a shaped hole proposed to the gas turbine community as a new baseline with which other geometries may be compared, other investigations may be benchmarked, and other CFD studies may be validated.

Measurements of adiabatic effectiveness at low and high density ratio showed that the baseline shaped hole had a wider coolant distribution at high density ratio for the same blowing ratio as compared with the low density ratio. Lateral spreading of coolant from the baseline shaped hole was highly dependent on the blowing ratio. At blowing ratios above 1.5, effectiveness distributions narrowed with increased blowing ratio. Narrowing of the coolant distributions coincided with a shallow decay rate of laterally-averaged effectiveness with downstream distance. The peak effectiveness for the low and high density ratio cases occurred near a blowing ratio of 1.5.

Multiple geometric parameters for shaped holes influence their performance. One useful metric for shaped hole performance is area-averaged effectiveness as a function of coolant flowrate per pitch, which scales the cooling performance of most shaped holes at low flowrates. In comparing the baseline shaped hole to other shaped holes in literature at high flowrates, it is clear that cooling differences are quite pronounced. A conservative hole expansion of the baseline shaped hole presented in this paper resulted in a cooling performance that was lower than some aggressively-expanded shaped holes.

Increasing the freestream turbulence to a moderate intensity did result in a widening of the jets at the intermediate to high blowing ratios. Area-averaged effectiveness decreased slightly with moderate turbulence at low blowing ratios, but not significantly for high blowing ratios.

## ACKNOWLEDGMENTS

The authors would like to acknowledge collaboration with David Bogard and Emily Boyd at the University of Texas at Austin. Support for this study was provided by the NASA Aeronautics Scholarship Program. Specifically, the authors would like to thank James Heidmann and Mark Celestina at NASA for their guidance. The authors also would like to thank machinist Phil Irwin for careful machining of the film cooling holes.

## REFERENCES


[1] Bunker, R. S., 2005, "A Review of Shaped Hole Turbine Film Cooling Technology," *J. Heat Transfer*, **127**(4), pp. 441-453.

[2] Barigozzi, G., Benzoni, G., Franchini, G., and Perdichizzi, A., 2006, "Fan-Shaped Hole Effects on the Aero-Thermal Performance of a Film Cooled Endwall," *J. Turbomach.*, **128**(1), pp. 43-52.

[3] Gritsch, M., Colban, W., Schär, H., and Döbbeling, K., 2005, "Effect of Hole Geometry on the Thermal Performance of Fan-Shaped Film Cooling Holes," *J. Turbomach.*, **127**(4), pp. 718-725.

[4] Kohli, A. and Bogard, D. G., 1999, "Effects of Hole Shape on Film Cooling With Large Angle Injection," ASME International Gas Turbine and Aeroengine Congress, 99-GT-165.

[5] Saumweber, C. and Schulz, A., 2012, "Effect of Geometry Variations on the Cooling Performance of Fan-Shaped Cooling Holes," *J. Turbomach.*, **134**(6), pp. 061008.

[6] Heneka, C., Schulz, A., Bauer, H., Heselhaus, A., and Crawford, M. E., 2012, "Film Cooling Performance of Sharp Edged Diffuser Holes With Lateral Inclination," *J. Turbomach.*, **134**(4), pp. 041015.

[7] Liu, J. S., Malak, M. F., Tapia, L. A., Crites, D. C., Ramachandran, D., Srinivasan, B., Muthiah, G., and Ventkataramanan, J., 2010, "Enhanced Film Cooling Effectiveness With New Shaped Holes," Proc. ASME Turbo Expo, GT2010-22774.

[8] Hyams, D. G. and Leylek, J. H., 2000, "A Detailed Analysis of Film Cooling Physics: Part III—Streamwise Injection With Shaped Holes," *J. Turbomach.*, **122**(1), pp. 122-132.

[9] Lu, Y., 2007, "Effect of Hole Configurations on Film Cooling from Cylindrical Inclined Holes for the Application to Gas Turbine Blades," Ph.D. Dissertation, Louisiana State University.

[10] Dorrington, J. R., Bogard, D. G., and Bunker, R. S., 2007, "Film Effectiveness Performance for Coolant Holes Embedded in Various Shallow Trench and Crater Depressions," Proc. ASME Turbo Expo, GT2007-27992.

[11] Sargison, J. E., Oldfield, M. L. G., Guo, S. M., Lock, G. D., and Rawlinson, A. J., 2005, "Flow Visualization of the External Flow from a Converging Slot-Hole Film-Cooling Geometry," *Experiments in Fluids*, **38**(3), pp. 304-318.

[12] Kusterer, K., Bohn, D., Sugimoto, T. and Tanaka, R., 2007, "Double-Jet Ejection of Cooling Air for Improved Film Cooling," *J. Turbomach.*, **129**(4), pp. 809-815.

[13] Kusterer, K., Tekin, N., Reiners, F., Bohn, D., Sugimoto, T., Tanaka, R., and Kazari, M., 2013, "Highest-Efficient Film Cooling by Improved Nekomimi Film Cooling Holes—Part 1: Ambient Air Flow Conditions," Proc. ASME Turbo Expo, GT2013-95027.

[14] Moser, S., Ivanisin, M., Woisetschläger,, J., and Jericha, H., 2000, "Novel Blade Cooling Engineering Solution," ASME International Gas Turbine and Aeroengine Congress, 2000-GT-0242.

[15] Liu, C., Zhu, H., Bai, J., and Xu, D., 2012, "Experimental and Numerical Investigation on the Film Cooling of Waist-Shaped Slot Holes Comparing with Converging Slot Holes," *J. Turbomach.*, **134**(1), pp. 011021.

[16] Okita, Y. and Nishiura, M., 2007, "Film Effectiveness Performance of an Arrowhead-Shaped Film-Cooling Hole Geometry," *J. Turbomach.*, **129**(2), pp. 331-339.

[17] Heidmann, J. D. and Ekkad, S., 2008, "A Novel Antivortex Turbine Film-Cooling Hole Concept," *J. Turbomach.*, **130**(3), pp. 031020.

[18] Colban, W., Thole, K. A., and Haendler, M., 2008, "A Comparison of Cylindrical and Fan-Shaped Film Cooling Holes on a Vane Endwall at Low and High Freestream Turbulence Levels," *J. Turbomach.*, **130**(3), pp. 031007.

[19] Gao, Z., Narzary, D. P., and Han, J-C., 2009, "Film-Cooling on a Gas Turbine Blade Pressure Side or Suction Side with Compound Angle Shaped Holes," *J. Turbomach.*, **131**(1), pp. 011019.

[20] Ai, W., Murray, N., Fletcher, T. H., Harding, S., Lewis, S., and Bons, J. P., 2012, "Deposition Near Film Cooling Holes on a High Pressure Turbine Vane," *J. Turbomach.*, **134**(4), pp. 041013.

[21] Schroeder, R. P. and Thole, K. A., 2013, "Shaped Hole Literature Review Database," Penn State Experimental and Computational Convection Laboratory (ExCCL), Web, <http://www.mne.psu.edu/psuexccl/>.

[22] Colban, W., Thole, K. A., and Bogard, D., 2011 "A Film Cooling Correlation for Shaped Holes on a Flat-Plate Surface," *J. Turbomach.*, **133**(1), pp. 011002.

[23] Thole, K. A., Sinha, A. K., Bogard, D. G., and Crawford, M. E., 1992, "Mean Temperature Measurements of Jets with a Crossflow for Gas Turbine Film Cooling Application," Rotating Machinery Transport Phenomena, J. H. Kim and W. J. Yang, ed., Hemisphere Publishing Corporation, New York.

[24] Haven, B. A., Yamagata, D. K., Kurosaka, M., Yamawaki, S., and Maya, T., 1997, "Anti-Kidney Pair of Vortices in Shaped Holes and Their Influence on Film Cooling Effectiveness," ASME International Gas Turbine and Aeroengine Congress, 97-GT-45.

[25] auf dem Kampe, T., Völker, S., Sämel, T., Heneka, C., Ladisch, H., Schulz, A., and Bauer, H.-J., 2013, "Experimental and Numerical Investigation of Flow Field and Downstream Surface Temperatures of Cylindrical and Diffuser Shaped Film Cooling Holes," *J. Turbomach.*, **135**(1), pp. 011026.

[26] Thole, K., Gritsch, M., Schulz, A., and Wittig, S., 1998, "Flowfield Measurements for Film Cooling Holes With Expanded Exits," *J. Turbomach.*, **120**(2), pp. 327-336.

[27] Lutum, E., von Wolfersdorf, J., Weigand, B., and Semmler, K., 2000, "Film Cooling on a Convex Surface with Zero Pressure Gradient Flow," *International*

*Journal of Heat and Mass Transfer*, **43**(16), pp. 2973-2987.

[28] Saumweber, C. and Schulz, A., 2012, "Free-Stream Effects on the Cooling Performance of Cylindrical and Fan-Shaped Cooling Holes," *J. Turbomach.*, **134**(6), pp. 061007.

[29] Davidson, F. T., Bruce-Black, J. E., Bogard, D. G., and Johns, D. R., 2008, "Adiabatic Effectiveness on the Suction Side of a Turbine Vane and the Effects of Curvature at the Point of Film Injection," Proc. ASME Turbo Expo, GT2008-51350.

[30] Bogard, D. G. and Thole, K. A., 2006, "Gas Turbine Film Cooling," *J. Propulsion and Power*, **22**(2), pp. 249-270.

[31] Bons, J. P., MacArthur, C. D., and Rivir, R. B., 1996, "The Effect of High Free-Stream Turbulence on Film Cooling Effectiveness," *J. Turbomach.*, **118**(4), pp. 814-825.

[32] Saumweber, C., Schulz, A., and Wittig, A., 2003, "Free-Stream Turbulence Effects on Film Cooling With Shaped Holes," *J. Turbomach.*, **125**(1), pp. 65-73.

[33] Fawcett, R. J., Wheeler, A. P. S., He, L., and Taylor, R., 2012, "Experimental Investigation Into Unsteady Effects on Film Cooling," *J. Turbomach.*, **134**(2), pp. 021015.

[34] Gritsch, M., Schulz, A., and Wittig, S., 1998, "Adiabatic Wall Effectiveness Measurements for Film Cooling Holes With Expanded Exits," *J. Turbomach.*, **120**(3), pp. 549-556.

[35] Gritsch, M., Schulz, A., and Wittig, S., 2000, "Film Cooling Holes With Expanded Exits: Near-Hole Heat Transfer Coefficients," *International Journal of Heat and Fluid Flow*, **21**(2), pp. 146-155.

[36] Gritsch, M., Schulz, A., and Wittig, S., 1998, "Discharge Coefficient Measurements for Film Cooling Holes With Expanded Exits," *J. Turbomach.*, **120**(3), pp. 557-563.

[37] Gritsch, M., Schulz, A., and Wittig, S., 2003, "Effect of Internal Coolant Crossflow on the Effectiveness of Shaped Film Cooling Holes," *J. Turbomach.*, **125**(3), pp. 547-554.

[38] Eberly, M. K. and Thole, K. A., 2014, "Time-Resolved Film Cooling Flows at High and Low Density Ratios," *J. Turbomach.*, **136**(6), pp. 061003.

[39] Figliola, R. S., and Beasley, D. E., 2006, *Theory and Design for Mechanical Measurements*, John Wiley & Sons, Inc., Hoboken, NJ.

[40] Roach, P. E., 1987, "The Generation of Nearly Isotropic Turbulence by Means of Grids," *International Journal of Heat and Fluid Flow*, **8**(2), pp. 82-92.

[41] Pichon, Y., 2009, "Turbulence Field Measurements for the Small Windtunnel," TTCRL Report, University of Texas at Austin.

[42] Harder K. J., and Tiederman W. G., 1991, "Drag Reduction and Turbulent Structure in Two-Dimensional Channel Flows," *Phil. Trans. R. Soc. Lond. A*, **336**(1640), pp. 19-34.